Dyer and Sotiropoulou *Herit Sci (2017) 5:24*
DOI 10.1186/s40494-017-0137-2

Heritage Science

RESEARCH ARTICLE

Open Access

A technical step forward in the integration of visible-induced luminescence imaging methods for the study of ancient polychromy

Joanne Dyer[1*] and Sophia Sotiropoulou[2]

Abstract

Photo-induced luminescence imaging techniques, such as UV-induced visible luminescence (UVL) and the more recently developed technique of visible-induced infrared luminescence (VIL), have been invaluable for the study of ancient polychromy, allowing the detection and mapping of luminescent materials, such as varnishes, consolidants, organic binders, and crucially, traces of pigments, organic and inorganic, that are often not visible to the naked eye. In the context of works from the Hellenistic period onwards, the detection of two pigments, Egyptian blue and rose madder lake, has been particularly pivotal in advancing the field. Current conventional methodologies for the digital mapping of these two luminescent pigments rely on the separate application of two techniques (VIL and UVL), each requiring a different illumination source and acquisition set-up. In this study, a novel approach is proposed, combining the use of visible-induced infrared luminescence and visible-induced visible luminescence to locate these two pigments. As the source of illumination in both cases is the same system of LEDs, the set-up has the advantage of requiring only minor filter changes between luminescence modes. The increased portability and safety compared to the use of methodologies that employ UV radiation represent notable advantages of this integrated system. The interchangeability between highly selective excitation sources, also significantly simplifies the experimental set-up and the need to adjust the object or equipment between acquisitions, ensuring better reproducibility of the data acquired and facilitating any post-processing procedures. This results in a user-friendly methodology for both experts and non-specialists alike. Three Hellenistic period terracottas; two from Canosa di Puglia, Italy (270–200 BC) and one from Myrina, Turkey (c. 100 BC), all characterised by large well-preserved areas of decoration in Egyptian blue and red lake, were studied in order to trial the approach. Comparisons were made with the more standard techniques of VIL and UVL, and it was shown that the combined method proposed efficiently detects and maps both of these pigments with analogous results to those obtained by more established methodologies. The observations made from the multispectral images acquired were verified by analysis of small samples of the pigments, using FTIR and Raman spectroscopy and HPLC-DAD analysis.

Keywords: Multispectral photoluminescence imaging, Ancient polychromy, VIL, VIVL, UVL, Hellenistic painted decoration, Egyptian blue, Madder lake, Terracotta, Colour calibration

*Correspondence: jdyer@britishmusuem.org
[1] Department of Scientific Research, The British Museum, Great Russell St, London WC1B 3DG, UK
Full list of author information is available at the end of the article

Background

In recent years, the study of polychromy on ancient sculpture, either free standing or from architectural contexts, has evolved into an interdisciplinary field, which by in-depth examination of these works of art, seeks to reconsider the production and decoration of antique sculpture, throughout a better understanding of the materials and techniques employed [1, 2]. The approach is one which brings together scientific findings, a reappraisal of ancient literature sources and historical and aesthetic insights, to reconsider the original appearance of antique sculpture, in which colour is no longer a hostile but essential component [3–5].

In archaic and classical sculptural works, the study of polychromy often refers to the detection of traces of original paint, gilding and/or organic media [3]. However, in Hellenistic times, polychromy gains its literal meaning, as in terms of aesthetic value, the colourful aspect of sculptural works from this period often rivals, if not prevails, over the form itself. A rich colourful corpus representing the polychrome appearance of Hellenistic sculptures, though not equivalent in several aspects with the marble large scale sculptures [6], is that of the terracotta figurines known as «Ταναγραίες» from the Boeotian Site of Tanagra, where they were discovered [7]. Although the technical traits for the manufacture of the terracotta statuettes were developed in Athenian workshops in the 5th and 4th century BC, by the last quarter of the 4th century BC onward, the Boeotian workshops, made a decisive step forward in introducing a new style, unfolding an infinite repertoire of naturalistic features, elegant postures and gestures, fine, freely-moving draperies and elaborate ornaments on the garments, embellished with a bright floral palette typical of feminine grace [8]. The development of the painted decoration on a matt, but still luminous and highly reflective (chiefly kaolinitic) white ground, applied after firing, was a key factor for the enrichment of the palette in hue, saturation and brightness. The privileged use of a pair of colours in the adornment of Tanagra figurines; Egyptian blue and rose pink, chiefly in the form of a madder lake, could be considered a signature of a purely Hellenistic style [6, 9, 10].

The contribution of multispectral imaging to the study of the three-dimensional polychrome objects is of great importance, either in the detection of pigment traces or in the mapping of colours on more intact surfaces, as it provides preliminary but well-defined information on the distribution of paint remains for further investigation [11]. Additionally, and complementarily to analytical data, it yields conclusive evidence on the techniques of application of these pigments, and can reveal mixtures or layering effects, which are pivotal both to the reconstruction of the original appearance of the object and to our understanding of artistic practices in antiquity [12].

Multispectral images, processed and registered as layers over a high resolution photograph in the visible, constitute an accurate record of the surviving original paint remains or subsequent restoration that, when compared to the present state of the object, may help to rediscover lost details. The ability to create false colour visualisations from these images can be particularly useful in this respect. In some cases, the availability of multispectral images to juxtapose with watercolour reconstruction proposals and artists' depictions of the 19th–early 20th centuries can also be extremely valuable. Although not always accurate, these renderings may include information that was present on the object at the time that they were painted but no longer survives or they may record alterations made at other points in their history. Comparison with multispectral images can either reinforce evidence for lost details or aid in dispelling these as artistic interpretations or later additions [11, 13].

Of the available multispectral imaging techniques for the study of ancient polychromy, photo-induced luminescence imaging, traditionally, UV fluorescence, or more correctly, UV-induced visible luminescence (UVL) imaging [14], has shown particular promise [12, 15]. The more recent development of the visible-induced infrared luminescence (VIL) imaging technique, and its successful application for the screening of Egyptian blue in numerous studies of archaeological and museum objects since 2009, [12, 15, 16], has also had a significant impact on the field. The advantage of both techniques lies in their high sensitivity, which can allow the detection of traces often not visible to the naked eye and their ability to offer a more holistic overview of the distribution of luminescent materials, such as varnishes, consolidants, organic binders and colorants, in the case of UVL [17–19], and of Egyptian blue pigment, in the case of VIL. In many cases, the eye is then able to interpolate from the luminescence of even a few remaining grains of material or pigment and partially reconstruct the lost fragments, giving clues towards the original appearance of the object. Although these fragmentary remains may also be detectable under the microscope, their discovery in isolation does not lend itself to the visualisation of the whole, as afforded by these images.

In the study of Hellenistic sculpture, either large-scale marble or small-scale terracotta, both these photo-induced luminescence imaging techniques find equivalence, as the mapping of its defining pigments; Egyptian blue (using VIL) and rose organic pigments, such as madder lake (using UVL), are of equal importance to the visualization of the whole [20]. However, current conventional methodologies for the digital mapping of these two luminescent pigments rely on the separate application of these two techniques, as each requires a different illumination source and acquisition set-up [13, 21].

Recently parallel efforts by various researchers have been made to integrate the two techniques into one set-up. In some cases, different lighting technologies, such as flashtubes [22], lasers [23] or systems borrowed from forensics, such as the CrimeScope®, have been employed[1], but the excitation wavelength ranges remain similar to the conventional methodologies. Another approach is to not only vary the illumination source but also the wavelength of light used to excite the luminescent species. Visible-induced visible luminescence (VIVL) imaging techniques, which record the emission of light in the visible region from a subject, when this is illuminated with visible light, have been proposed as a useful method for the mapping of luminescent materials, whilst circumventing the issues related to the use of UV lamps [24]. The methodology can use filtered sources[2] but is most efficient when it employs the more selective and intense irradiation provided by LED sources [24]. The application of such sources for the characterisation of the spatial distribution of red and yellow lake pigments using the VIVL technique, as an alternative to UVL, has been investigated [24], and was the subject of research carried out as part of the EU funded FP7 programme CHARISMA[3] project [14].

This work presents a selection of those results and extends it by proposing an integrated methodology, which adapts and combines the now well-known set-up for the VIL technique, with the VIVL technique as an alternative approach toward the simultaneous screening of visible and infrared emitting luminescent pigments, such as red lakes and Egyptian blue.[4]

The advantages of these techniques, which employ LEDs as their excitation sources, are discussed further in the forthcoming sections and provide a practical alternative to other set-ups developed on the same principle [23, 24]. Although powerful, such set-ups often have the draw-back of being based on custom-made systems (e.g. using lasers as excitation sources) that are not always accessible or affordable to the those in the cultural heritage/museums sector.

The true test of the approach however, lies in the ability to demonstrate that the combined VIL/VIVL method proposed is able to detect and map both of the pigments of interest, with results corresponding to those obtained by separately applying the more established VIL and UVL methodologies. To this end, and to highlight the particular suitability of this integrated method to the study of sculpture from the Hellenistic period, three terracottas from the collections at the British Museum were chosen; two from Canosa di Puglia, Italy (270–200 BC) and one from Myrina, Turkey (c. 100 BC), all of which are characterised by large well-preserved areas of decoration in Egyptian blue and red lake.

VIL and VIVL images, as well as UVL images for comparison, were recorded for all three objects and are initially appraised 'as shot'. Two filters for the acquisition of the VIVL images are evaluated. In addition, the effect of illumination with red LEDs versus white LEDs on the resultant VIL images is considered. The assessment is made on the efficacy of the proposed method to detect and accurately map each pigment. To verify the observations made from the multispectral images, small samples of each area of interest were taken and analysed, using FTIR and Raman spectroscopy and HPLC-DAD analysis, to identify the pigments present.

Additional assessment of the method is made by considering the intensity and colour information of the luminescence recorded by these images, particularly the VIVL images when compared to images acquired using the UVL technique. The advantages and limitations of the VIVL technique, particularly when probing the relationship between luminescence properties and molecular composition/biological source of the lake pigment, are discussed further.

Finally, practical post-processing tools based on established methodologies for the correction of luminescence images and open-source image processing software are proposed, which address some of the limitations identified and provide a means to visualise and evaluate the combined VIL/VIVL approach and their interpretation in the context of the Hellenistic works studied.

Methods

Objects

Three terracottas from the collections at the British Museum were chosen for this study:

Terracotta A (Fig. 1); a statuette of a woman with duck and conch shell (1846,0925.34), from Canosa di Puglia, Italy (270–200 BC). Areas of purple and blue over a white ground dominate the chiton and garland worn

[1] See for example: https://www.penn.museum/sites/artifactlab/tag/visible-induced-ir-luminescence/. Accessed 03/01/2017; https://uclagettyprogram.wordpress.com/tag/crimescope/. Accessed 03/01/2017; https://www.penn.museum/sites/artifactlab/2016/01/15/appear-project-multispectral-imaging-on-the-fayum-mummy-portraits/. Accessed 03/01/2017; http://cool.conservation-us.org/anagpic/2013pdf/anagpic2013_mallinckrodt_paper.pdf. Accessed 03/01/2017.

[2] See for example; https://www.penn.museum/sites/artifactlab/2016/01/15/appear-project-multispectral-imaging-on-the-fayum-mummy-portraits/. Accessed 03/01/2017.

[3] Cultural Heritage Advanced Research Infrastructures: Synergy for a Multidisciplinary Approach to conservation and restoration (Grant Agreement 228330).

[4] This work was presented at the 2012 Round Table on Ancient Sculptural Polychromy held at the Liebieghaus Skulpturensammlung, Frankfurt am Main on the 13th–14th September, 2012. The meeting report, including an abstract of the presentation given, can be found here: http://www.glyptoteket.dk/sites/default/files/trackingcolour-4.pdf.

Fig. 1 Terracotta A—a statuette of a woman with duck and conch shell (1846,0925.34), and the locations of the samples taken for microanalysis, as listed in Table 1

by the woman depicted in this piece. Her hair is a brick red/orange, with areas of a darker red/orange observed around the hairline. She holds a duck with pink wings and underbelly in her left hand. Height 40.64 cm.

Terracotta B (Fig. 2); a group of two female figures sitting on a couch (1885,0316.1), from Myrina, Turkey (c. 100 BC). The two female figures are depicted sitting on a couch covered in blue and pink drapery. The lady on the right wears a pink chiton and covers herself in a sheer himation. Her brick red/orange hair is a gathered in a low bun. She leans into the lady on the left who is wearing a white chiton, which exposes her right shoulder and breast, and a himation pulled over her head. Red/orange shoes are observed to peep from under the pink hemline of her clothing. Height 21.0 cm.

Terracotta C (Fig. 3); an oinochoe in the form of a female head, with a figure of Niké (1846,0925.26.a), from Canosa di Puglia, Italy (270–200 BC). The figure of the winged Niké atop the head of a lady is clothed in a purple and blue chiton. The petalled garland and wings are also decorated in these hues. She holds a bird in her right hand and is flanked by two garlanded heads. The female head which forms the main body of the vessel also wears such a garland or stephané of pointed leaves, with some of these appearing a warmer tone of pink than on the Niké's chiton. The iris of both eyes and lips are coloured a brick red/brown. Blue particles are visible in the whites of the eyes. Height 85.09 cm.

These were investigated by the multispectral photoluminescence and microanalytical techniques described below. For microanalysis small samples of a few grains were taken with a scalpel from each area of interest, as recorded in Figs. 1, 2, 3.

Multispectral imaging techniques

The experimental set-up for the acquisition of the multispectral images described in this work can be considered as being made up of a number of equipment components:

- A pair of radiation sources, providing the incident radiation to the object being studied and in the case of luminescence techniques also providing the means to induce the luminescence (the excitation source) in the materials under study.
- A filter or set of filters in order to allow the transmission of radiation in the wavelength range under study and exclude unwanted radiation from being recorded.
- A detector or recording device.
- A set of standards to enable comparability and the application of post-processing methods.

The recording device and standards remain constant throughout. All images were taken using a modified Canon 40D camera body. The modification consists of the removal of the inbuilt UV-IR blocking filter, in order to exploit the full sensitivity of the CMOS sensor (c. 350–1100 nm), which has a maximum resolution of 3888 × 2592 (10.1 megapixels). The lens used is a Nikon AF NIKKOR 50 mm F/1.8D lens, which was used at its widest F-stop setting (1.8) in order to record all the luminescence images with shutter speeds in the range

Fig. 2 Terracotta B—a group of two female figures (perhaps Demeter and Persephone) sitting on a couch (1885,0316.1), and the locations of the samples taken for microanalysis, as listed in Table 1

between 0.5 and 5 s. The selection of the wavelength range under investigation is achieved by placing a filter or a set of filters in front of the lens. The camera is operated in fully Manual mode with the picture style set to 'Neutral' and an ISO speed of 100 (or lowest setting available). White balance is set to 'Custom', except for the acquisition of UV-induced visible luminescence images, when it is set to a colour temperature setting of 6500 K.

Colour calibration and luminance correction is carried out by acquisition using the RAW file format and the application of post-processing procedure, details of which are given below. This image correction procedure requires that an X-rite (or "Macbeth") Colorchecker® and a reference grey scale, comprising a set of Lambertian black, grey and white tiles, are placed close to and in the same plane as the object under investigation. These Spectralon® references have uniform reflectance properties across the ultraviolet, visible and infrared spectral ranges under investigation and show no luminescence properties.[5] The combination of radiation source and filter (or sets of filters) is altered to allow the study of the spectral windows of interest. These are discussed more specifically below within the requirements of each particular technique. For a more detailed description of the techniques and workflows for the optimised and standardised acquisition of these images, refer to the recently published manual on multispectral imaging techniques [14]. The total weight of the combined set-up is approximately 7 kg.

Visible-induced visible luminescence imaging (VIVL)

The excitation is provided by two identical high power LED (red, green and blue) light sources (Eurolite LED PAR56 RGB spots 20 W, 151 LEDs, beam angle 21°) of which the blue LEDs ($\lambda_{max} = 465$ nm) are used exclusively for the acquisition of VIVL images. The two light sources can optionally be connected to a DMX console, which transforms the RGB spots into a tunable LED source, where the Red, Green and Blue LEDs can be used separately or mixed and their intensity can be controlled in a continuous manner. The radiation sources are symmetrically positioned at approximately 45° with respect to the focal axis of the camera and at about the same

[5] https://www.labsphere.com/site/assets/files/2628/spectralon_diffuse_reflectance_standards.pdf. Accessed 8 May 2017.

Fig. 3 Terracotta C—an oinochoe in the form of a female head, with a figure of Niké (1846,0925.26.a), and the locations of the samples taken for analysis, as listed in Table 1

distance from the object as the camera (Fig. 4a). For the objects investigated in this work, this distance ranged from 1 to 2 m, depending on the object. An IDAS-UIBAR bandpass filter (400–700 nm) and either a Lee No. 21 (50% transmission at 560 nm) or a Lee No. 16 (50% transmission at c. 540 nm) polyester filter are placed in front of the camera lens, in order to block the incident blue light and investigate the range of interest (c. 520–700 nm for the IDAS-UIBAR and Lee No. 21 filter combination and c. 475–700 nm for the IDAS-UIBAR and Lee No. 16 filter combination, see Fig. 4a for transmittance curves).

Visible-induced infrared luminescence imaging (VIL)

The excitation is provided by the LED sources described above but switching to the red LEDs ($\lambda_{max} = 630$ nm), which are used exclusively for the acquisition of VIL images (Fig. 4b). A Schott RG830 cut-on filter (50% transmittance at c. 830 nm) is placed in front of the camera lens, in order to block off the visible component and investigate the emission of IR radiation in the 800–1100 nm region (see Fig. 4b for transmittance curves). In the monochrome VIL images, materials that emit IR radiation are recognisable as 'bright white' areas in the image [25].

Visible images and more conventional ultraviolet-induced visible luminescence (UVL) images were also acquired for comparison to the VIVL and VIL images, which form the focus of this work, and to aid in post-processing procedures for the standardisation and calibration (see below). Both are well-known techniques but for a more detailed description of the workflows for the optimised and standardised acquisition of these images, see the manual on multispectral imaging techniques, [14].

Visible-reflected imaging

The object is illuminated by two photographic Classic Elinchrom 500 Xenon flashlights equipped with a softbox (diffuser) and symmetrically positioned at approximately 45° with respect to focal axis of the camera and at about the same height. An interference UV-IR blocking filter IDAS-UIBAR filter (bandpass, c. 380–700 nm) is placed in front of the camera lens.

Ultraviolet-induced visible luminescence imaging (UVL)

The excitation is provided by two identical Wood radiation sources (365 nm) filtered with a Schott DUG11X interference bandpass filter (280–400 nm). The emission of the radiation sources is a relatively sharp line centred at 365 nm. The radiation sources are symmetrically positioned at approximately 45° with respect to the focal axis of the camera. A Schott KV418 cut-on filter (50% transmission at c. 418 nm) and an IDAS-UIBAR bandpass filter (400–700 nm) are placed in front of the camera lens,

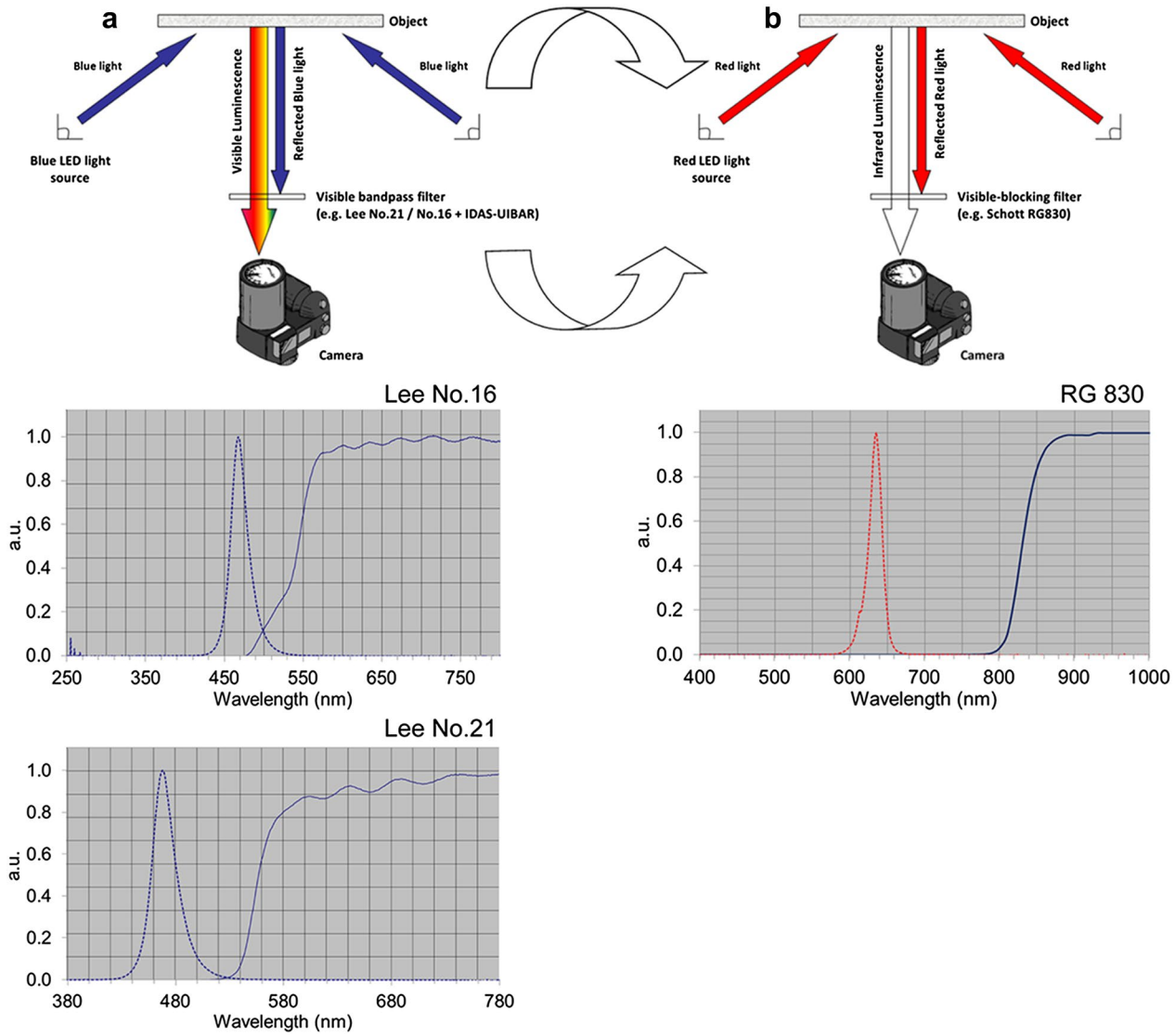

Fig. 4 Schematic representation of the experimental set-up for the collection of **a** visible-induced visible luminescence (VIVL) and **b** visible-induced infrared luminescence (VIL) images. The plots below each set-up show the LED excitation source output and the transmittance curves of filters used in front of the camera in each case

in order to investigate the visible range (420–700 nm) [21].

All images are acquired as RAW images with a maximum resolution of 3888 × 2592 (10.1 megapixels) and transformed into 3888 × 2592 pixel resolution images in 16-bit TIF (tagged image file) format, by applying a set of recommended presets which turn-off all enhancements (e.g. recovery, fill light, blacks, contrast, brightness, clarity, vibrance, saturation, as well as setting the tone-curve to linear). This procedure can be carried out using the camera software or external programs such as Adobe Photoshop. For further details on the conversion of images from RAW, see the manual on multispectral imaging techniques, [14].

Post-processing procedures for the standardisation and calibration of the VIS, UVL and VIL images are then carried out using "BM_workspace", a plug-in for Nip2, the open-source graphical user-interface of VIPS, a free image processing software, [26]. For details on how to download BM_workspace and the Nip2 software, as well as descriptions, workflows and data requirements for the post-processing of these images, see the manual on multispectral imaging techniques [14]. Note that, although at present BM_workspace does not currently accommodate

the post-processing of VIVL images, alternatives not involving the use of the BM_workspace are presented in the "Discussion" section.

Microanalytical techniques

FTIR Spectroscopy was performed on a Nicolet 6700 spectrometer attached to a Continuum IR microscope equipped with MCT/A detectors. The sample was analysed in transmission mode, flattened in a diamond microcompression cell. The cell was opened and the flattened sample supported on one diamond window, a clean area of which was used for background spectra. The field of view was controlled by the sliding aperture which, when fully open, gives a maximum area of analysis of 100 × 100 μm. The spectra were acquired over a range of 4000–650 cm^{-1} using 32 scans at a resolution of 4 cm^{-1} and automatic gain and were identified by comparison with in-built databases.

Raman spectroscopy was carried out using a Jobin–Yvon LabRam Infinity spectrometer using green (532 nm) and near IR (785 nm) lasers with maximum powers of 2.4 and 4 mW at the sample respectively, a liquid nitrogen cooled CCD detector and an Olympus microscope system. Samples of a few grains were collected using a clean scalpel, placed onto a microscope slide and measured without any further treatment. The resultant spectra were identified by comparison with a British Museum in-house database.

For HPLC-DAD analysis the samples were extracted in dimethyl sulfoxide (DMSO, 10 min at 80 °C) and 0.5 M oxalic acid/acetone/water/methanol mixture (1:30:40:30) (15 min at 80 °C). The combined extracts for each sample were dissolved in DMSO/water/methanol (2:1:1).

Analyses were carried out using a Hewlett-Packard (now Agilent) HPLC HP1100 system comprising a vacuum solvent degasser, a binary pump, autosampler and column oven. The column used for the separation was a Luna C18(2) 100 Å, 150 × 2.0 mm, 3 μm particle size (Phenomenex) stabilized at 40 °C in the column oven. Detection was performed using an HP1100 DAD with a 500 nL flow cell and using detection wavelengths from 200 to 700 nm. The solvent system used comprised two solvents: (A) 99.9% water/0.1% trifluroacetic acid (v/v); and (B) 99.9% acetonitrile/0.1% trifluroacetic acid (v/v). The elution programme was a first gradient from 95% A/5% B to 70% A/30% B over a period of 25 min followed by a second linear gradient to 100% B after a further 15 min. After 10 min elution with pure B, a third linear gradient was used to return to the initial composition (95% A/5% B) in 15 min. The flow rate was fixed throughout at 0.2 mL per/minute creating a system back-pressure of 120 bars (12.0 MPa).

Results

The multispectral images acquired from Terracottas A, B and C (Figs. 5, 6 and 7) are discussed in the following sections.

In each figure, (a) and (b) show the visible-reflected (VIS) and UV-induced visible luminescence (UVL) images, which are used as a comparison to the visible-induced visible luminescence (VIVL) images shown in (c) and (d). The visible-induced infrared luminescence (VIL) images acquired are shown in (e) and (f). The UVL/VIVL and VIL images shown in Figs. 5, 6 and 7 are given 'as shot', for the purpose of comparison, while selected

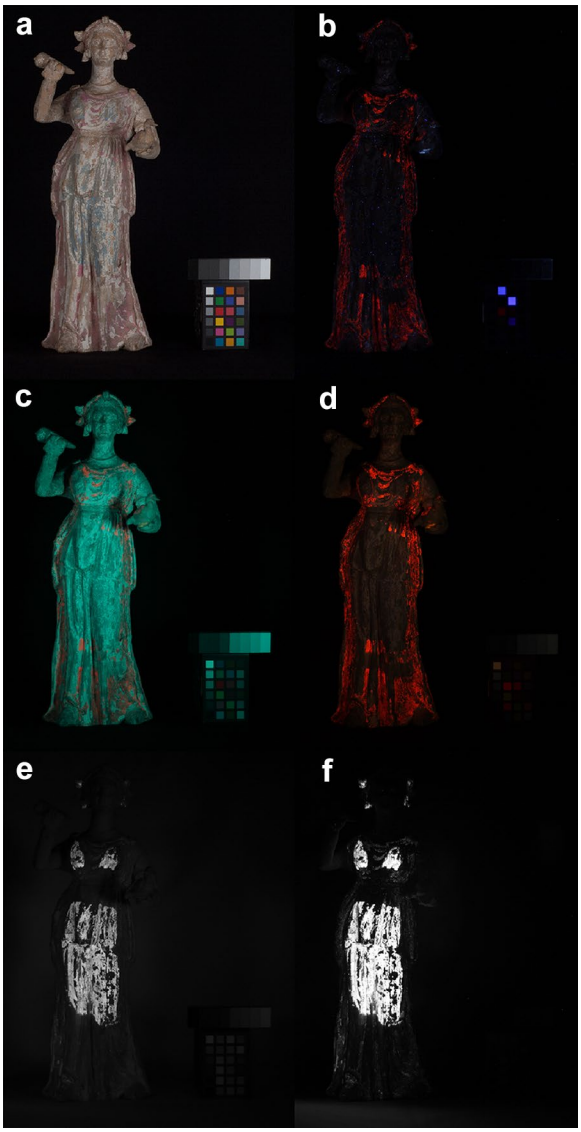

Fig. 5 **a** Visible-reflected (VIS); **b** UV-induced visible luminescence (UVL); **c**, **d**, visible-induced visible luminescence (VIVL); **e**, **f**, visible-induced infrared luminescence (VIL) images taken of Terracotta A

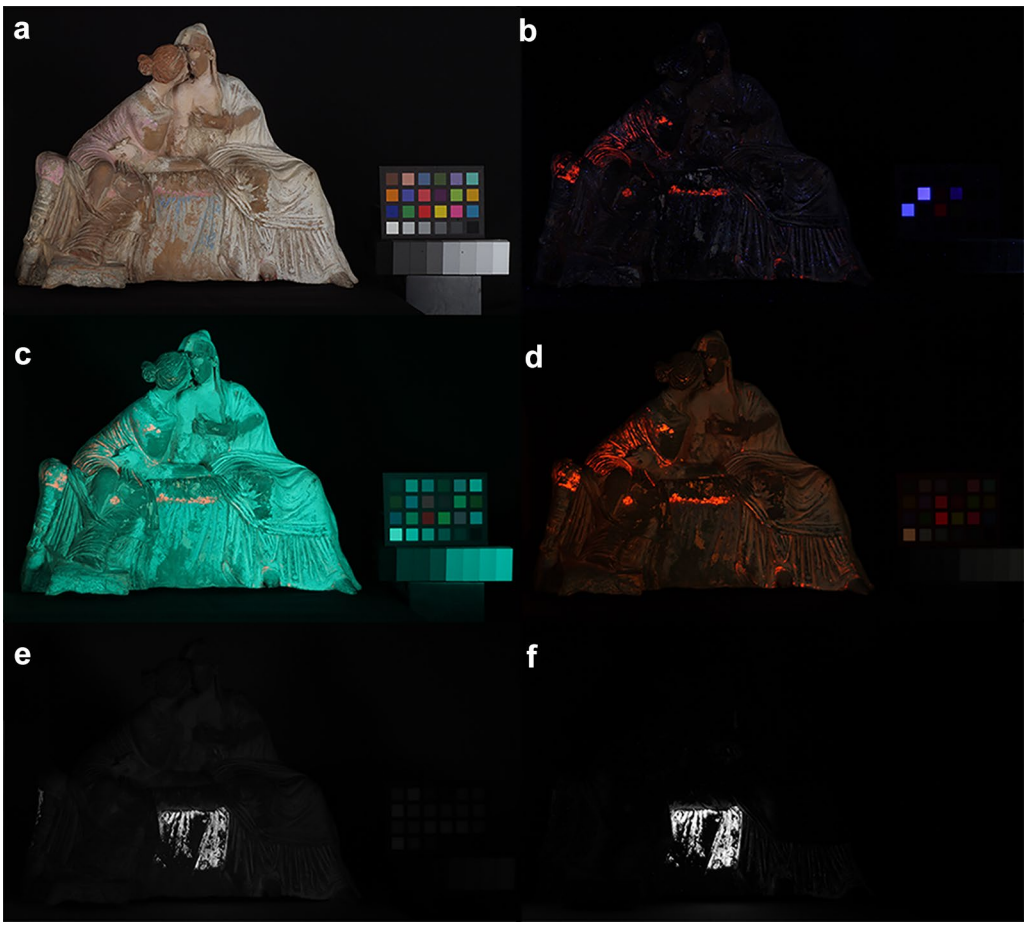

Fig. 6 **a** Visible-reflected (VIS); **b** UV-induced visible luminescence (UVL); **c**, **d**, visible-induced visible luminescence (VIVL); **e**, **f**, visible-induced infrared luminescence (VIL) images taken of Terracotta B

images after post-processing are presented in Figs. 11, 12 and 13, in the "Discussion" section.

Comparing UVL and VIVL images

Areas of bright pink-orange luminescence, as are usually associated with luminescence from red lake pigments, such as madder lake, were observed in the UVL images for all three of the objects investigated. In Fig. 5b, this is localised to areas of the figure's chiton and garland, and some areas of the duck's wings and head. In Fig. 6b, this luminescence is confined to areas on the figures' garments (particularly the figure on the proper right, although some is also observed along the edges of the chiton worn by the figure on the proper left) and the couch. In Fig. 7b, the luminescence is observed on areas of the wings and the chiton worn by figure of Niké and on several of the pointed leaves on the stephané worn by the female head, as well as around the eyes. Comparison of these images with their corresponding visible images (Figs. 5, 6, 7a), shows that the luminescence observed in all three cases is concomitant with the regions of pink or purple pigment present on these objects.

Figure 5, 6 and 7c, d show the visible-induced visible luminescence (VIVL) images taken of each of the terracotta objects, using blue LED illumination and the IDAS-UIBAR plus the Lee Nos. 16 and 21 filters placed in front of the camera lens, respectively.

In all the VIVL images acquired, a good correlation is observed between the luminescence associated with the areas of pink or purple pigment observed on the UVL images and the luminescence observed in the VIVL images. In the VIVL images captured using the Lee No. 16 filter (Figs. 5, 6, 7c), the luminescence associated with these areas appears pink-orange, but the filter allows too much reflected blue light into the camera, as is apparent from the 99% tile of the Spectralon® reference scale in these images. This causes the images to appear very blue and decreases the contrast between the emitted and reflected radiation. Although some reflected light is also present in the VIVL images captured using the Lee No.

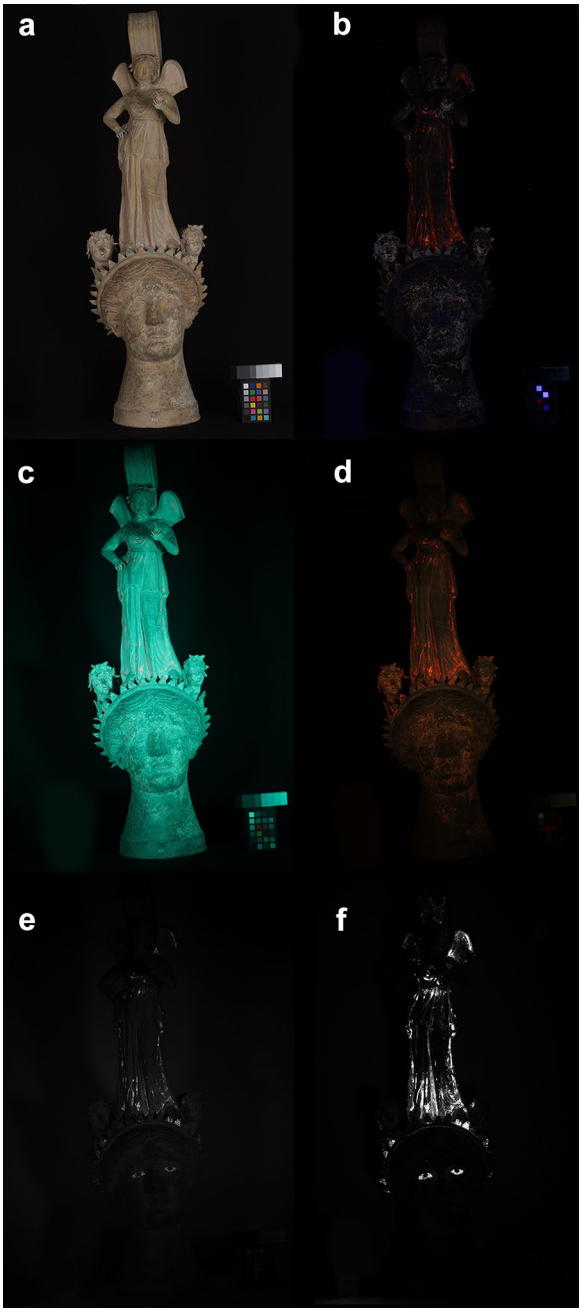

Fig. 7 **a** Visible-reflected (VIS); **b** UV-induced visible luminescence (UVL); **c**, **d**, visible-induced visible luminescence (VIVL); **e**, **f**, visible-induced infrared luminescence (VIL) images taken of Terracotta C

21 filter (Figs. 5, 6, 7d), the contrast between the luminescence recorded, and the reflected light is comparable to that observed in the UVL image, however the luminescence appears more orange in these VIVL images.

It should be noted that areas of blue luminescence are also observed in the UVL images. These mostly correspond to particles of dust on the surface of the object and a small amount of stray light, as may be observed from the 99% tile of the Spectralon® reference scale in these uncorrected images. However, the UVL image of Terracotta A (Fig. 5b), also shows an area of blue luminescence under the belly of the duck (Fig. 8b). As this corresponds to an area of pink pigment (Fig. 8a), it is likely that we are observing luminescence from a consolidant in this area of pigment which is masking the emission from the red lake. The corresponding area in the VIVL images (Fig. 8c, d), appears yellow and orange, respectively. This effect is addressed further in the "Discussion" section.

VIL images

The visible-induced infrared luminescence (VIL) behaviour in each of the above cases was investigated by switching to red LED illumination and replacing the filter in front of the camera lens with a visible blocking filter, as described (Fig. 4). In addition, comparisons were made to the images obtained using white illumination provided by simultaneously switching on red, green and blue (RGB) LEDs.

In all three of the objects investigated, bright white luminescence was observed suggesting the presence of Egyptian blue [25]. In Fig. 5e, f, this is localized to the areas of blue pigment on the figure's chiton and garland. In Fig. 6e, f, VIL was observed restricted to the areas of blue pigment on the couch. In Fig. 7e, f, luminescence was noted on areas of the wings and the chiton worn by figure of Niké, as well as in the whites of the eyes of the female head and on several of the pointed leaves on the stephané worn by the latter.

Comparison of the images obtained with red LED (Figs. 5, 6, 7e) vs. RGB illumination (Figs. 5, 6, 7f), demonstrates that, although the intensity of the luminescence is of course increased by using all three LED wavelengths, the images are qualitatively the same. In cases where there was little pigment present, the intensity of the red LED could be increased or RGB illumination used.

Microanalysis

The presence of red lake pigments and Egyptian blue, suggested from the luminescence observed in the images discussed above, was further investigated by microanalysis of small samples taken from each area of interest. However, as these two pigments are part of a more extensive colour palette used to create the polychrome finish of these terracotta pieces, representative samples from other areas of surviving polychromy were also taken for each of the three objects investigated. The areas of interest were recorded in the detail images obtained with the VMS-004D 400× USB Microscope (see Additional file 1).

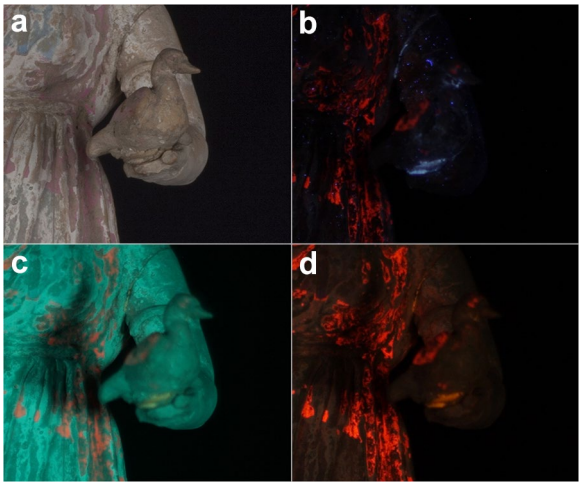

Fig. 8 Detailed images of the duck in Terracotta A. **a** visible-reflected (VIS); **b** UV-induced visible luminescence (UVL); **c**, **d**, visible-induced visible luminescence (VIVL), taken with Lee No. 16 and No. 21 filters, respectively

FTIR and Raman spectroscopy were employed to investigate the samples taken from these locations. Samples of the pink/purple areas were also taken for HPLC-DAD analysis.

The samples are labelled by terracotta and the number of the sample, e.g. A1, describes sample 1 for Terracotta A. The locations of the samples taken from terracotta A, B and C are given in Figs. 1, 2 and 3, respectively. Detailed images of these locations are provided in the Additional file 1. All other results are summarised in Table 1 and described by object below.[6]

Terracotta A

Analysis of a sample (A1, Fig. 1) from an area of purple drapery above the right foot, showed the presence of pink particles, suggestive of a madder lake. The FTIR spectrum shows the lake substrate to be an amorphous hydrated alumina with characteristic features of Al-O lattice vibrations at c. 660 cm^{-1} and other broad bands due to coordinated water at c. 3400 and 1650 cm^{-1}. The presence of colorants derived from madder was confirmed by HPLC-DAD analysis, which found peaks with matching retention times to those of purpurin, pseudopurpurin/munjistin and to an unidentified component also seen in reference samples of madder dye and pigment. Alizarin was not detected.

[6] The spectral datasets supporting the conclusions of this article are archived in the British Museum Scientific Research data archives (Project No. 7529) and associated report [27], enquires for access should be directed to science@thebritishmuseum.ac.uk.

Madder lake pigments containing high proportions of the colorants, purpurin and/or pseudopurpurin, but little or no alizarin, are typical of the "rose madders" associated with objects from antiquity [28]. Alizarin, purpurin and pseudopurpurin differ in colour, with alizarin being more orange in colour. The relative proportion of the different components not only influences the colour of the resulting pigment, but also strongly influences its emission properties. Studies of the luminescence behaviour of alizarin, purpurin and pseudopurpurin as aluminium (Al^{3+}) complexes have shown that, whereas purpurin-Al^{3+} and pseudopurpurin-Al^{3+} complexes show emission maxima at 551/595 and 542/583 nm respectively, alizarin-Al^{3+} has an emission maximum at c. 640 nm and a fluorescence quantum yield nearly 50 times lower than the equivalent purpurin complex [29]. This is responsible for the characteristic pink–orange luminescence observed on UV excitation of madder lakes with high proportions of purpurin and/or pseudopurpurin, but little or no alizarin. However, although such assumption is precise, it cannot be argued based solely on the imaging results without analytical confirmation, as even if present, the emission from the alizarin compound would be overwhelmed by the high fluorescence quantum yield of the emission from the purpurin compounds. Additionally, when such composition is analytically confirmed, it is often suggested as evidence for the use of a madder lake prepared from *Rubia peregrina* L. (wild madder) not the cultivated variety *Rubia tinctorum*, [30]—pp. 112–113, 122–123, [31]. However, other factors such as the harvesting, storage conditions and age of the plants, have been shown to affect the dyestuff composition in the root [31–34] and the preparation procedure can significantly modify the original dyestuff composition in the resulting dye or pigment [28, 31, 35]. In addition, the relative proportions of the compounds that are detected upon analysis are also dependent on the extraction method and analytical procedure chosen [36]. As a result, the unequivocal identification of the *Rubia* species used to prepare the madder pigment in this sample is not straightforward from the evidence at hand.

In addition, a few glassy blue particles were noted amongst the pink particles in the sample from the area of purple drapery, together with white particles identified by FTIR spectroscopy as kaolinite from the bands present at 3698, 3622, 1117, 1031, 1009 and 914 cm^{-1}. The latter are likely particles of the ground as these were also identified in the sample (A2, Fig. 1) from a white area of the chiton near the right foot. The glassy blue particles were also observed in a sample (A3, Fig. 1) from an area of blue drapery over the left knee. These were identified by both FTIR and Raman spectroscopy as Egyptian blue, with bands at 1161, 1056, 1002, 755 and 665 cm^{-1} in the

Table 1 Summary of the results of FTIR, Raman and HPLC analyses of samples taken from Terracottas A–C

Sample	Material analysed	Analytical results		
		FTIR	Raman	HPLC
Terracotta A—statuette of a woman with duck and conch shell (1846,0925.34)				
A1 Purple pigment	Pink particles	Amorphous hydrated alumina (attributed to the lake substrate)		Purpurin, pseudopurpurin/munjistin (attributed to organic colorants derived from madder, likely from *Rubia* spp.)
	Blue particles		Egyptian blue	
	White particles	Kaolinite (attributed to the ground layer)		
A2 White pigment/ground	White particles	Kaolinite (attributed to the ground layer)		
A3 Blue pigment	Blue particles	Egyptian blue Quartz Calcite	Egyptian blue	
A4 and A5 Red/orange pigment	Red and yellow particles	Red Ochre Quartz Gypsum	Hematite (red particles) Goethite (yellow particles)	
	White particles	Kaolinite (attributed to the ground layer)		
Terracotta B—group of two female figures sitting on a couch (1885,0316.1)				
B1 White pigment/ground	White particles	Kaolinite Alunite (attributed to the ground layer) Gypsum		
B2 Red/orange pigment	Deep red particles		Cinnabar	
	Red/orange particles	Iron oxide Quartz	Hematite	
	White particles	Kaolinite Alunite (attributed to the ground layer) Gypsum		
B3 Blue pigment	Blue particles	Egyptian blue	Egyptian blue	
B4 Flesh tone pigment	Red particles		Hematite	
	White particles	Kaolinite Alunite (attributed to the ground layer) Gypsum		
B5 Pink pigment	Pink particles	Amorphous hydrated alumina (attributed to the lake substrate)		Purpurin, pseudopurpurin/munjistin (attributed to organic colorants derived from madder, likely from *Rubia* spp.)
	White particles	Kaolinite Alunite (attributed to the ground layer)		
B6 Red/orange pigment	Red particles	Red ochre	Hematite	
	Yellow particles	Goethite	Goethite	
	Black particles		Amorphous carbon	
	White particles	Kaolinite Alunite (attributed to the ground layer)		
B7 Black pigment	Black particles		Amorphous carbon	
	White particles	Quartz Kaolinite (attributed to the ground layer)		

Table 1 continued

Sample	Material analysed	Analytical results		
		FTIR	Raman	HPLC
Terracotta C—oinochoe in the form of a female head (1846,0925.26.a)				
C1 White pigment	Blue particles	Egyptian blue		
	White particles	Gypsum Kaolinite (attributed to the ground layer)		
C2 Red/brown pigment	Dark red particles		Cinnabar	
	White particles	Calcite Gypsum Kaolinite (attributed to the ground layer)		
C3 Purple pigment	Pink particles	Amorphous hydrated alumina (attributed to the lake substrate)		Purpurin, pseudopurpurin/munjistin (attributed to organic colorants derived from madder, likely from *Rubia* spp.) Flavokermesic acid (attributed to organic colorant from an insect source)
	Blue particles	Egyptian Blue		
	White particles	Gypsum (attributed to the ground layer)		
C4 Blue pigment	Blue Particles	Egyptian Blue		
	White particles	Gypsum (attributed to the ground layer)		
C5 White/ground	White particles	Calcite Gypsum Kaolinite (attributed to the ground layer)		
C6 Pink pigment	Deep red particles		Cinnabar	
	White particles	Calcite Gypsum (attributed to the ground layer)		
C7 Dark purple (blackened red) pigment	Deep red particles		Cinnabar	
	White particles	Calcite Gypsum Kaolinite (attributed to the ground layer) Quartz		

Sample locations are detailed Figs. 1, 2, 3

FTIR spectrum. Thus it appears that some Egyptian blue was added to the madder lake pigment in order to modify the pink hue of the garment to a cooler tone. Despite its low quantity, evidence for this addition can be observed by comparison of the VIL and UVL/VIVL images (Fig. 9), where even single particles of the blue pigment can be observed in the VIL image in the area of purple drapery where this sample was taken (Fig. 9e).

Mixtures of red and yellow particles were observed in the samples taken from the hair (A4 and A5, Fig. 1). FTIR analysis of these showed the presence of ochre, quartz and gypsum, as well as kaolinite from the ground, in both samples. Additionally, Raman spectroscopy identified the red and yellow particles as hematite and goethite, respectively.

Terracotta B

FTIR analysis of a sample (B1, Fig. 2) of the white chiton taken from the left knee of lady on the left, showed this to be mainly composed of kaolinite and alunite, with bands at 3486, 1227, 1079 and 681 cm^{-1} identifying the later. Bands consistent with a small amount of gypsum were also observed at 3410 and 1621 cm^{-1}. Kaolinite and alunite are presumed to be the main constituents of the ground as they were also found by FTIR analysis of the other samples taken from this piece. The exception was

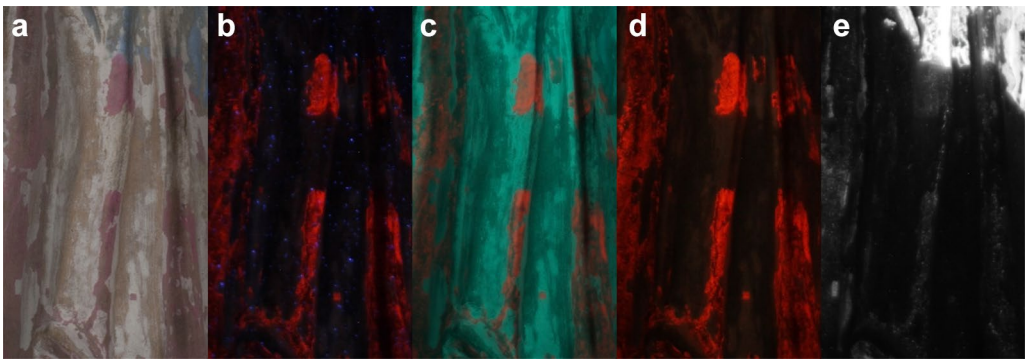

Fig. 9 Detailed images of the garment in Terracotta A. **a** Visible-reflected (VIS); **b** UV-induced visible luminescence (UVL); **c**, **d**, visible-induced visible luminescence (VIVL), taken with Lee No. 16 and No. 21 filters, respectively; **e** visible-induced infrared luminescence (VIL)

the sample (B3, Fig. 2) from the blue drapery covering the area of the couch between the ladies, where both FTIR and Raman spectroscopy identified Egyptian blue, but only the glassy blue particles were analysed in this case.

In the sample (B2, Fig. 2) from the right red/orange shoe of lady on the left, a large amount of jagged deep red and some red/orange particles were observed together with some white and colourless particles. The latter were identified as the kaolinite/alunite ground together with some gypsum from FTIR analysis. In addition, bands at 799 and 780 cm^{-1}, and 1425 and 1037 cm^{-1} respectively, were observed suggesting the presence of quartz, calcite and aluminosilicate compounds, which as secondary minerals often associated with a red ochre, are perhaps indicative of its presence. This was confirmed by Raman analysis of the sample which identified hematite bands at 224, 291, 406, 500 and 611 cm^{-1} due to the red/orange particles. The large jagged deep red particles were found to be cinnabar from the Raman shift bands at 353, 342, 290, 277 and 253 cm^{-1}.

Hematite was also identified by Raman analysis as the very few red particles present in the flesh tone coloured sample (B4, Fig. 2) taken from the top of left thumb of the lady on the left. However, the sample was dominated by the presence of white particles found by FTIR analysis to be kaolinite from the bands at 3698, 3622, 1117, 1032, 1008 and 914 cm^{-1}, together with some alunite and gypsum.

In the sample (B5, Fig. 2) of pink pigment from the drapery over right arm of seat, the clumps of pink particles were analysed by FTIR spectroscopy. The FTIR spectrum shows the lake substrate in this case was also an amorphous hydrated alumina from the features observed at c. 3400 1650 cm^{-1} and c. 660 cm^{-1}. The presence of colorants derived from madder was confirmed by HPLC-DAD analysis, which found peaks with matching retention times to those of purpurin, pseudopurpurin/munjistin and to an unidentified component also seen in reference samples of madder dye and pigment. As in the previous sample from Terracotta A, alizarin was not detected.

The red/orange pigment from the hair of lady on the right (B6, Fig. 2) was found to be composed of large deep red, yellow and black particles, which were identified by Raman spectroscopy as hematite, goethite and amorphous carbon, respectively. The off-white particles which were also observed in this sample were identified from FTIR analysis as the kaolinite/alunite ground. Evidence for hematite and goethite was also observed from this FTIR spectrum, with bands at 3142, 894 and 805 cm^{-1} evident for the latter.

Finally, the black particles (B7, Fig. 2) sampled from the area at the base of the couch by the lady on the right's feet were identified by Raman spectroscopy as amorphous carbon. The sample also contained white particles found to be a mixture of kaolinite and quartz from FTIR analysis.

Terracotta C

FTIR analysis of a sample (C1, Fig. 3) from an area of the white of the right eye, where these blue particles are visible, identified Egyptian blue to be present from bands at 1269, 1160, 1060, 995, 755 and 665 cm^{-1}. In addition evidence for gypsum and kaolinite was also observed at 1032, 1008, 914 cm^{-1} and 3522, 3406, 1685, 1621, 1136, 671 cm^{-1}, respectively. As this mixture was also found in the FTIR analysis of the other samples taken from this piece, gypsum and kaolinite are likely the main constituents of the ground. However in addition to the ground, the sample (C5, Fig. 3) taken from the right cheek of the small head to the left of the female head also contains the white pigment calcite, which dominates the FTIR spectrum of this sample with bands at 2516, 1797, 1414, 876 and 714 cm^{-1}.

Egyptian blue was also found to be present by FTIR analysis as the blue pigment in the sample (C4, Fig. 3)

from the chiton of the figure of Niké; the large glassy blue particles were also accompanied by some gypsum.

As was the case with Terracotta A, the sample (C3, Fig. 3) of purple pigment analysed from the bottom of chiton of the figure of Niké (near the right foot), also contained some glassy blue particles among the pink particles. These were identified by FTIR spectroscopy as Egyptian blue. As previously, evidence for the addition of this pigment to modify the hue of the lake pigment can be observed by comparison of the VIL and VIVL images (Fig. 10), where the luminescence in both images is observed to overlap in the area of purple drapery where this sample was taken. The pink particles were identified by FTIR spectroscopy as a madder lake with an amorphous hydrated alumina lake substrate, as with the samples from the previous two pieces. However, upon HPLC-DAD analysis in addition to peaks with matching retention times to those of purpurin, pseudopurpurin/munjistin and to an unidentified component also seen in reference samples of madder dye and pigment (as previously alizarin was not detected), a peak with matching retention time and UV–visible spectrum to flavokermesic acid was identified. This suggests that a mixture of red colorant sources may have been employed in the manufacture of this pigment. Recent reports have shown that insect sources, namely Armenian cochineal (*Porphyrophora hameli* Brandt) were used in mixtures with madder on Hellenistic period terracottas found in Thessaloniki [37]. By contrast, analysis of the warmer-coloured sample of pink pigment (C6, Fig. 3) taken from the central pointed leaf of the stephané, did not show the presence of organic colorants. The small deep red particles colouring this sample were analysed by Raman spectroscopy and found to be cinnabar. Evidence for gypsum and calcite were also found by FTIR analysis of the sample from bands at 3406, 1621, 1136, 670 cm^{-1} and 1420, 879 cm^{-1}, respectively. The presence of cinnabar was also found from the Raman analysis of samples from two other areas; the dark red colour taken from the top lip of the female head (C2, Fig. 3) and the dark purple taken from the lips of the small head to her right (C7, Fig. 3) from the bands at 353, 342, 290, 277 and 253 cm^{-1}. In addition, FTIR analysis showed calcite, gypsum and kaolinite to be present in both samples, with some additional bands for quartz at 800 and 782 cm^{-1} observed in the spectrum of sample C7.

In summary, microanalysis of the samples taken from the three objects investigated confirm the presence of madder lake, prepared from *Rubia* spp., and Egyptian blue as suggested from the UVL/VIVL and VIL images, respectively. In addition, these investigations have shown that the cooler toned pinks or purple tones observed in two of the objects (Terracotta A and C) are in fact mixtures of these two pigments. Evidence for this can be seen by comparing the UVL/VIVL and VIL images, where even single particles of the blue pigment can be observed in the VIL image in the areas where these samples were taken. In one of these cases (Terracotta C), the mixture also contained an additional pink colorant, likely to be derived from an insect source.

The analytical data has also provided details about the lake pigment substrate, which in all three cases investigated appears to be an amorphous hydrated alumina. In some archaeological pigments from this period, substrates containing both calcium sulphate (in the form of gypsum) and amorphous hydrated alumina have been found, suggesting addition of a calcium carbonate source (in the form of powdered chalk or cuttlefish bone) as an alkaline ingredient, which subsequently transforms to gypsum on reaction with the alum solution [28]. However, no evidence of gypsum in the substrates to suggest that the lake pigments in this study were manufactured by this method was found.

The study has also looked at the wider palette present which is comprised of red and yellow ochres, carbon black, cinnabar, calcite and gypsum on kaolinite grounds, consistent with Hellenistic period terracottas [10] and decorated ceramics.

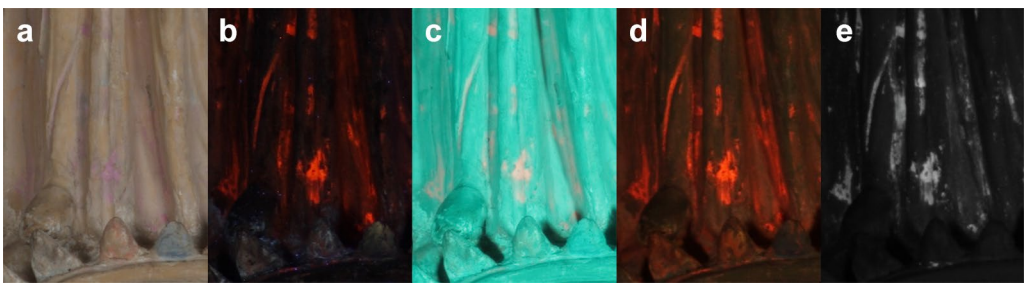

Fig. 10 Detailed images of the garment in Terracotta C. **a** Visible-reflected (VIS); **b** UV-induced visible luminescence (UVL); **c**, **d**, visible-induced visible luminescence (VIVL), taken with Lee No. 16 and No. 21 filters, respectively; **e** visible-induced infrared luminescence (VIL)

Discussion

Assessment of method

The proposed method offers a practical alternative for the simultaneous screening of red lakes and Egyptian blue using a single set-up and RGB illumination source. This study has shown that the combined VIL/VIVL method is able to detect and map both of these pigments with analogous results to those obtained by separately applying the more established VIL and UVL methodologies. This is particularly the case with the VIVL method using the Lee No. 21 filter (or equivalent), which produces images that are qualitatively comparable with UVL images.

The use of a methodology based on LED lighting also has several advantages, not least amongst which is the safety aspect to the user compared to the use of illumination sources that produce UV radiation. As both the wavelength and intensity of the LED source can be selected, this also limits the exposure of the pieces under investigation to both harmful UV wavelengths and levels of radiation. The use of a DMX console connected to the RGB light sources is particularly useful in this respect, as it allows optimisation of the illumination via full control of the individual intensity of the Red, Green and Blue LEDs of both light sources in a synchronised manner.

In addition, the tunable LED wavelengths provide a more targeted excitation source than UV for the pigments of interest, which preferentially absorb in the visible range. All red lakes show a main absorption band in the 400–650 nm spectral range. For madder lakes this is centred at c. 455–540 nm, depending on their preparation procedure [38], the blue LED ($\lambda_{max} = 465$ nm) is an optimal excitation wavelength for these coloured species whilst avoiding the excitation of binders, varnishes or resins that preferentially absorb UV wavelengths. This not only increases the emission signal from the species of interest but the narrow emission band also minimises the effects of distortion of the emission features, such as self-absorption, multiple scattering and inner filter effects, produced by interference from other excited species [21, 39, 40]. Evidence of this can be seen by comparing the area of pink pigment under the belly of the duck in the UVL and VIVL (Lee No 21 filter) images of Terracotta A (Fig. 8b, d, respectively). As discussed above, the UVL image shows an area of blue luminescence but the corresponding area in the VIVL images is very similar in colour to that observed for the areas of purple pigment in the VIVL image. This suggests that in the UVL image we are observing luminescence from a species in this area of pigment that is masking the emission from the red lake and that this contribution is eliminated by the more targeted excitation and detection provided by the VIVL method.

The use of the red LED ($\lambda_{max} = 630$ nm) in the acquisition of VIL images is also an optimal excitation wavelength for the Egyptian blue chromophore, which has an absorption maximum at c. 630 nm and in combination with the RG830 cut-on filter, allows the collection of VIL images with no contribution from stray IR light.

The interchangeability between highly selective excitation sources, allowing the recording of both VIL and VIVL images by using the same irradiation source, also significantly simplifies the experimental set-up and the need to adjust the object or equipment between acquisitions. This increases the portability, affordability and accessibility of the set-up, which could be used in a museum environment as well as in situ on historic or archaeological sites. In addition, the simplified set-up ensures better reproducibility of the data acquired and facilitates any post-processing procedures, making this a user-friendly methodology for both experts and non-specialists.

Despite these notable advantages, several issues however remain to be addressed. The gel filters selected for the acquisition of VIVL images in this study have the advantage of being practical to use and affordable, however both have certain limitations.

The acquisition window of the Lee No. 21 filter (540–700 nm) is smaller in wavelength range but also lower in transmittance than the typical acquisition window for UVL images (420–700 nm, for the combination of the Schott KV418 cut-on and IDAS-UIBAR bandpass filters used in this study). This means that although the reflected light from the excitation source is largely excluded (as can be observed from the 99% tile of the Spectralon® reference scale in these images) and the contrast between the luminescence recorded and the reflected light is comparable to that observed in the UVL image, certain emission wavelengths (in the green/yellow range) are also significantly cut-off. Therefore, while the VIVL images captured using the No. 21 filter are efficient in mapping the distribution of the luminescent red lake pigments, the limited transmittance in the 540–700 nm window introduces a constraint for using this method to probe the relationship between luminescence properties and molecular composition of the lake pigment, where the differences in the emitted luminescence could be used for differentiating between red lakes from different biological sources. This would be particularly limiting where the emission characteristics present only slight differences, as is the case for madder vs. cochineal or kermes lake pigments [38], or in cases where the pigment is made up of a combination of colorants from different biological sources, as found for one of the sample of purple pigment (C3, Fig. 3) analysed in this study. The use of an adequate filter of wider and higher transmittance would increase the potential applicability of the method for screening (or making a preliminary distinction of) red lakes. Unfortunately, although

the Lee No. 16 filter, has a (slightly) larger acquisition window (approx. 475–700 nm) and higher transmittance, in this case, the higher transparency partly overlaps with the Blue LED emission spectrum and allows too much of the reflected light through from the illumination source (as is apparent from the 99% tile of the Spectralon® reference scale in these images). As a result, the uncorrected images appear very blue and the contrast between the emitted and reflected radiation is decreased. The effects of ambient stray light may be somewhat remedied by the choice of more efficient filters or by the application of stray light correction as part of the post-processing of the images. However, given that the range of possible acquisition windows for both UVL and VIVL images, may vary widely according to the particular properties of the experimental set-up chosen, the issue of colour calibration based on agreed standards is vital, in order to obtain set-up-independent, comparable results, which could reliably be used to distinguish luminescence emitted from different materials based on colour information. To address these issues, the application of post-processing techniques for the removal of stray light and colour calibration is invaluable.

The importance of post-processing in multispectral image interpretation is increasingly being recognised, both as a means to obtain the maximum information out of the images but also as a means to standardise images, to make them device-independent and allow them to be compared directly [14]. Post-processing procedures for the standardisation and calibration of the VIS, UVL and VIL images in this study were carried out using the BM_workspace, as described in the "Methods" section. However as the BM_workspace does not currently accommodate the post-processing of VIVL images, alternatives were explored in which emphasis was placed on comparability of the resulting data in terms of colour and usability of the post-processing methodology, whilst accepting that an absolute colour calibration of the images may not be possible.

Post-processing

Two approaches are suggested, using the images taken of Terracotta A as an example, which may be considered as complementary to each other rather than alternatives.

The 'as shot' images (Fig. 5b–d) record the colour information for the emitted luminescence in each case, as detected by the camera, but as discussed, the presence of stray light from the excitation source distorts the information and colour of the luminescence displayed in these images. Removal of the stray light can be carried out following previously published procedures, where the contribution of stray light on photo-induced luminescence images (ambient light, light emitted by other materials present in the room, parasitic light coming from the irradiation source), is appraised and taken into account by using the Spectralon® 99% reflectance standard [15, 24, 39]. This yields images which are very similar in terms of the luminescence observed from the areas of pink/purple pigment.

Figure 11a compares the images taken with the three different set-ups, after stray light correction. The first image from the left corresponds to the UVL image, presented 'as shot' in Fig. 5b, the middle image corresponds to the VIVL image taken with the Lee No. 16 filter, presented 'as shot' in Fig. 5c, and the image on the right corresponds to the VIVL image taken with the Lee No. 21 filter, presented 'as shot' in Fig. 5d. Although not strictly colour calibrated, the hue of the luminescence is very similar in each case and bears good chromatic resemblance to the colour calibrated UVL image [first from left in (Fig. 11a)]. It should be noted that the UVL image still has contributions from the blue and green channels (as expected) but in the VIVL images this has almost disappeared. In addition, the luminescence due to the pink pigment under the belly of the duck noted earlier is now "unmasked".

The above approach is useful in that it allows visualization of the hue but also of the intensity of the luminescence, which in certain cases, may be distinctive of the red lake [29]. To optimise the results of such an approach, albeit limited, the use of a series of commercial luminescent standards to allow colour and luminance calibration could be considered.[7] However, although a systematic investigation assessing the performance of the photo-induced luminescence images, in cross-validation with corresponding spectral data [24], has demonstrated that the approach is sufficiently sensitive and reliable for the detection and mapping of luminescent pigments directly on works of art, at present the direct characterisation of the natural source of the lake pigments based exclusively on imaging data, even when accurately calibrated, remains tenuous at best. This is particularly the case when considering that a pigment may be made up of a combination of colorants from different biological sources, as discussed earlier.

An alternative/complementary approach, which dispenses with the need for colour calibration, is to consider only the information contained in the red channel of these VIVL images. Figure 11b compares the red channels (converted to greyscale) extracted from each of the images shown in Fig. 11a. As may be observed, the similarity between these monochrome images is very high, adding to the argument that the VIVL approach

[7] See for example those developed by UV innovations—http://www.uvinnovations.com/.

is producing almost identical information to the UVL image where red lake location is concerned. Treating these images in a similar, and now familiar, way to how VIL images are currently considered, would provide a monochrome map of red lake pigment location. The production of a monochrome image also has the further advantage that it can be used in the creation of a false colour image, in which these pigment location maps can be overlaid. This would allow the simultaneous visualisation of areas of red lake and Egyptian blue pigment and perhaps any regions where these pigments co-exist as mixtures or overlays.

Figure 12 shows the monochrome images taken from the red channels of (a) the VIVL (taken using the Lee No. 21 filter) and (b) the VIL images of Terracotta A. The third image (Fig. 12c) shows an RGB false colour image created by overlaying these images, where the VIVL and VIL monochrome images are assigned as the R and G channel, respectively. The image was created using the image processing tools in the Nip2 software. Details of how to create this false colour image from the two monochrome images are given in Additional file 2.

Although comparison of the monochrome images is already suggestive of regions where both pigments co-exist (as even single particles of Egyptian blue can be observed in the VIL image in areas which also show emission from the red lake—compare Fig. 12a, b), the false colour image makes this comparison much more immediate (Fig. 12c). In addition, the processing tool allows flexibility as to which image is assigned to each channel, so that these can be easily interchanged to provide different visualisation of areas of overlap which may be enhanced by different colour combinations. Some of these may provide an indication of mixtures or overlays in the areas where the pigments occur together, as the overlap can attenuate the colour of the false colour image where the emission is most intense in that area. In the case of the image in Fig. 12c, the areas with strong intensity in the R channel, corresponding to emission from the lake pigment, are modulated to an orange colour by the presence of some intensity in the G channel corresponding to emission from the Egyptian blue particles in those areas. This would suggest the admixture of a relatively small amount of Egyptian blue particles, as was determined from analysis of the samples taken from these areas. Areas of strong intensity in either channel are not noticeably affected. Figure 13 shows the monochrome images taken from the red channels of (a) the VIVL (taken using the Lee No. 21 filter) and (b) the VIL images of Terracotta B, and (c) the false colour image created by overlaying these images, where the VIVL and VIL monochrome images are assigned as the R and G channel, respectively. In this case, no overlap between the areas with strong intensity in either the R or G channels is observed and neither channel appears to be attenuated in colour, suggesting no discernible admixture between the red lake and Egyptian blue pigments.

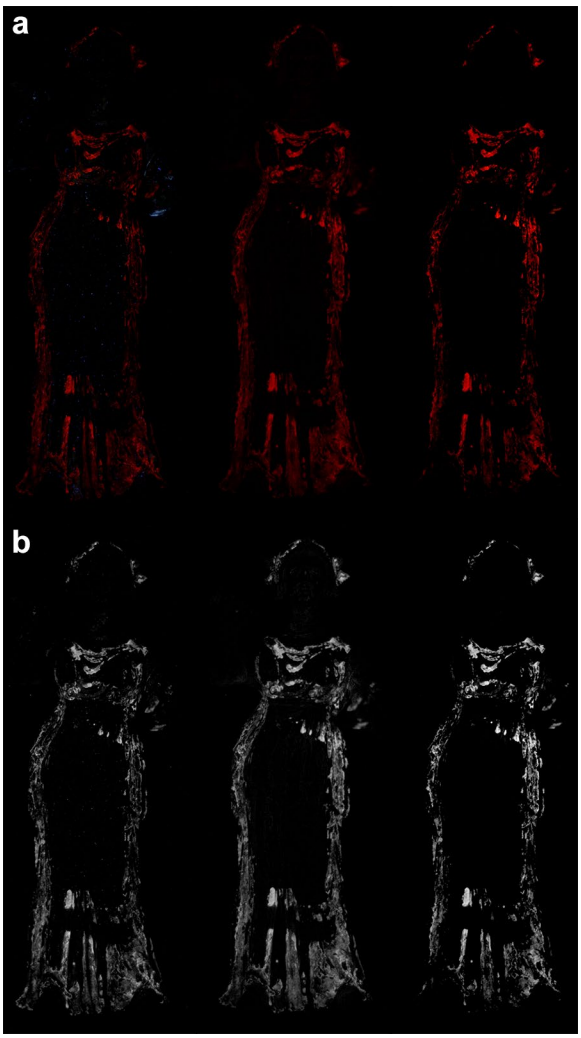

Fig. 11 From *left*: UV-induced visible luminescence (UVL); visible-induced visible luminescence (VIVL) using Lee No. 16; VIVL using Lee No. 21 images taken of Terracotta A **a** corrected (*stray light removed*), **b** red channel only (*converted to greyscale*). See the corresponding 'as shot' images presented in Fig. 5b–d

Caution must however be taken with such interpretations of these false colour images as evidence for the relative proportions of pigment present, as there is no direct relationship between the relative intensity or the colour coordinates of either channel and the relative ratio of the pigments. The intensities observed are not only proportional to the amounts of the pigment mapped but also to their relative luminescence quantum yields. Thus, the high luminescence quantum yield of the Egyptian

blue pigment would ensure that the intensity in whichever channel it is assigned would dominate in any overlay of images, unless present in very small quantities, as described for Fig. 12. To extract information on the relative content of pigments in a mixture based on the colour coordinates from a false colour image, the contribution from each channel would have to be scaled by a factor which took account of the relative luminescence quantum yields of the pigments mapped [41]. Such an approach would need to be based on quantitative spectral data, as has been demonstrated in the literature [15, 29], and could perhaps form the basis of a future study for the development of a post-processing tool to create false colour images that could more accurately represent the proportion of pigments used in mixtures or overlays.

Conclusions

This study proposes an alternative integrated methodology for the simultaneous screening of two pigments which are ubiquitous in the study of ancient polychromy, and in particular, the polychromy of the Hellenistic period; Egyptian blue and rose organic pigments, chiefly madder lake.

The approach, using a single set-up and only one illumination source, represents a significant simplification over most current methodologies which rely on the separate application of two techniques (VIL and UVL), each requiring a different illumination source. The case studies discussed in this investigation have shown that that the combined VIL/VIVL method proposed is able to efficiently detect and map both of these pigments with analogous results to those obtained by more established methodologies. In addition, the use of LED sources provide a more targeted excitation for the pigments of interest, reducing risk to both user and objects, and avoiding spurious signals from excited species produced by less specific forms of irradiation. The simplified set-up also promotes better data reproducibility and facilitates post-processing, enhancing the user-friendliness of the approach.

Efforts have also been made to mirror the accessibility of the acquisition set-up by offering practical post-processing tools based on established methodologies for the correction of luminescence images and open-source image processing software. The result is a set of alternative/complementary approaches towards the visualisation and evaluation of luminescence in VIL/VIVL

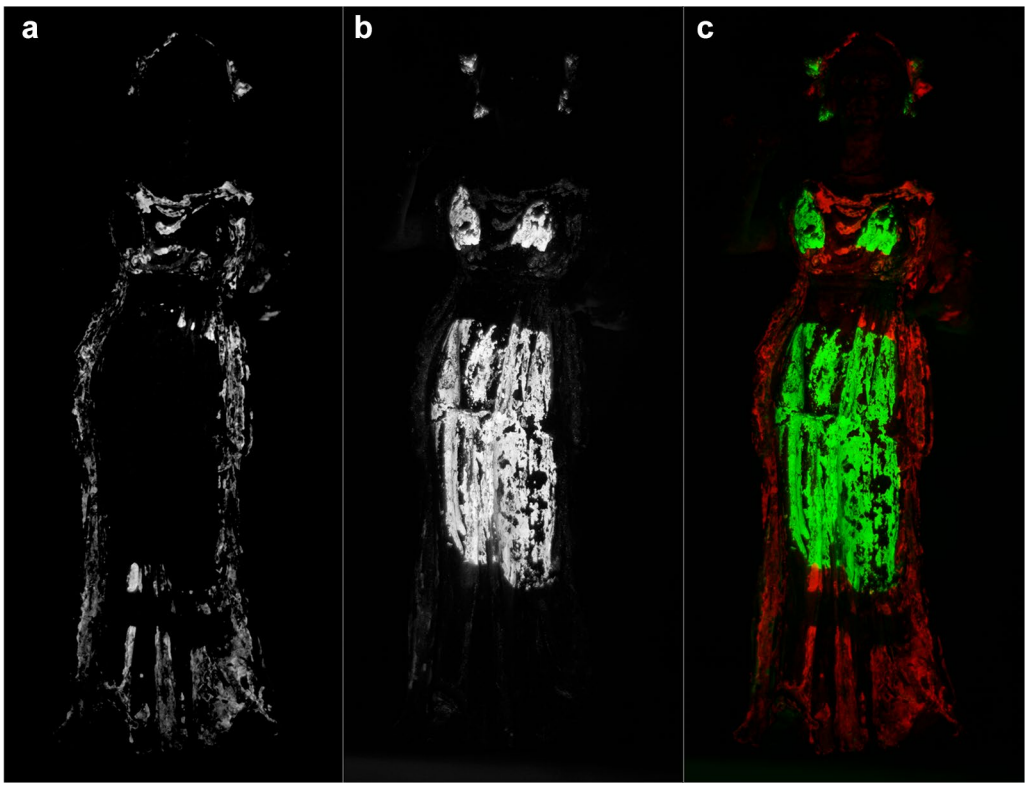

Fig. 12 The monochrome images taken from the red channels of **a** VIVL (taken using the Lee No. 21 filter) and **b** VIL images of Terracotta A **c** an RGB false colour image created by overlaying these images where the VIVL and VIL monochrome images are used as the R and G channel, respectively

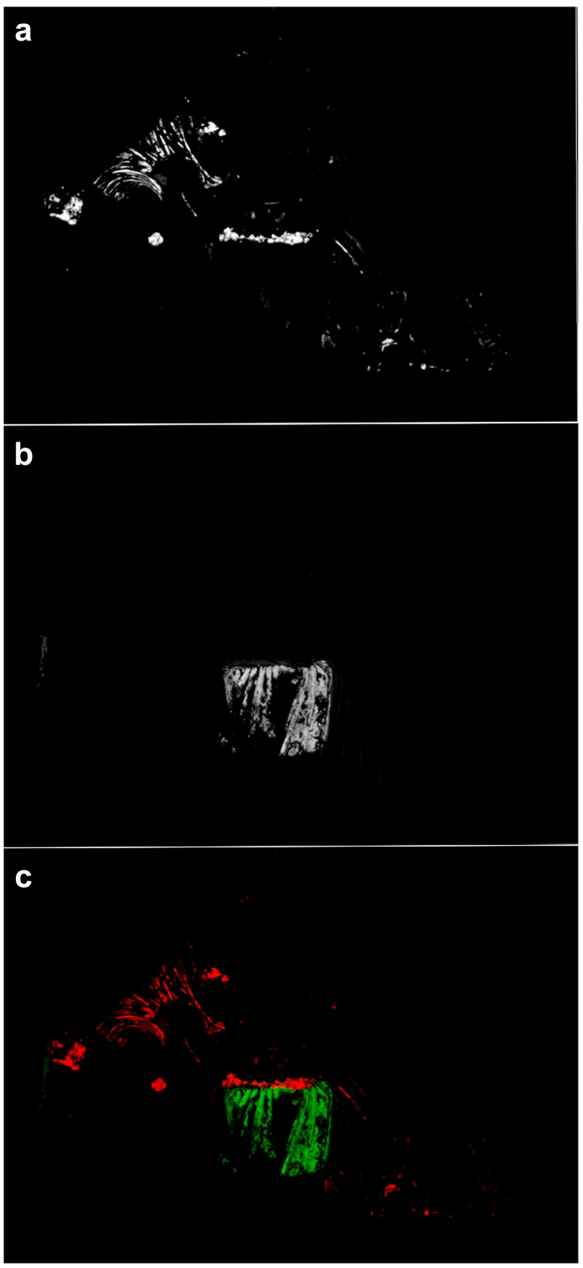

Fig. 13 The monochrome images taken from the red channels of **a** VIVL (taken using the Lee No. 21 filter) and **b** VIL images of Terracotta B; **c** an RGB false colour image created by overlaying these images where the VIVL and VIL monochrome images are used as the R and G channel, respectively

images, which allow these to be interpreted meaningfully and with an immediacy which circumvents the need for specialist knowledge. It is important to highlight that, in the case studies presented, the observations made from such an appraisal of these images have additionally been verified analytically, confirming not only the identities of both pigments investigated at the locations indicated by the luminescence images but, in some cases, also providing evidence for regions where these pigments co-exist as mixtures. The visualisations created, particularly those that overlay the monochrome images, are therefore more than just pigment maps but also evidence of the techniques used to create the polychrome finishes of the objects investigated. Although these methods are apposite *par excellence* to the study of Hellenistic sculpture, their wider applicability as a significant user-friendly contribution to the study of luminescent pigments is evident.

Additional files

Additional file 1. Detail images of the areas of interest sampled for microanalysis.

Additional file 2. Instructions for creating a false colour image from an overlay of the VIL/VIVL images in Nip2.

Abbreviations

UVL: ultraviolet-induced visible luminescence; VIL: visible-induced infrared luminescence; VIVL: visible-induced visible luminescence; LED: light-emitting diode; FTIR: Fourier transform infrared spectroscopy; HPLC-DAD: high-performance liquid chromatography, with diode-array detection.

Authors' contributions

JD and SS contributed to the conception of the study and acquisition and analysis of the data. These authors were involved in the interpretation of the results and drafting/revising of the manuscript. Both authors read and approved the final manuscript.

Author details

[1] Department of Scientific Research, The British Museum, Great Russell St, London WC1B 3DG, UK. [2] "ORMYLIA" Foundation, Art Diagnosis Centre, 63071 Ormylia, Chalkidiki, Greece.

Acknowledgements

The research leading to these results was partly funded by EU FP7 programme CHARISMA—Cultural Heritage Advanced Research Infrastructures: Synergy for a Multidisciplinary Approach to conservation and restoration (Grant Agreement 228330). The authors wish to thank John Cupitt for helpful discussions on the nip2 software and Antony Simpson for his help in preparing the figures for publication.

Competing interests

The authors declare that they have no competing interests.

Availability of data and materials

The datasets supporting the conclusions of this article are included within the article and its additional files. The raw datasets supporting the conclusions of this article are archived in the British Museum Scientific Research data archives (Project No. 7529), enquires for access should be directed to science@thebritishmuseum.ac.uk.

Funding

This work was partly funded by EU FP7 programme CHARISMA—Cultural Heritage Advanced Research Infrastructures: Synergy for a Multidisciplinary Approach to conservation and restoration (Grant Agreement 228330).

Publisher's Note

Received: 26 January 2017 Accepted: 24 April 2017
Published online: 19 June 2017

References

1. Brinkmann V, Primavesi O, Hollein M. Circumlitio the polychromy of antique and mediaeval sculpture. Frankfurt am Main: Liebieghaus Skulpturensammlung; 2010.
2. Bourgeois B. Arts and crafts of colour on the louvre tanagra figurines. In: Jeammet V, editor. Tanagras: figurines for life and eternity: the Musée du Louvre's collection of Greek figurines. Valencia: Fundación Bancaja; 2010. p. 238–44.
3. Østergaard JS, Nielsen AM, Stanford NM. Transformations: classical sculpture in colour. Copenhagen: Ny Carlsberg Glyptotek; 2014.
4. Panzanelli R. The color of life. Los Angeles: J. Paul Getty Museum; 2008.
5. Brinkmann V, Wünsche R. Gods in color—painted sculpture of classical antiquity. München: Biering & Brinkmann; 2007.
6. Blume C. When colour tells a story—the polychromy of hellenistic sculpture and terracottas. In: Brinkmann V, Primavesi O, Hollein M, editors. Circumlitio the polychromy of antique and mediaeval sculpture. Frankfurt am Main: Liebieghaus Skulpturensammlung; 2010. p. 144–65.
7. Jeammet V. The Origin of the tanagras: fourth century B.C. Athens—the origin and diffusion of tanagra figurines. In: Jeammet V, editor. Tanagras: figurines for life and eternity: the Musée du Louvre's collection of Greek figurines. Valencia: Fundación Bancaja; 2010. p. 4–11.
8. Jeammet V. Sculpture *en miniature*. In: Østergaard JS, Nielsen AM, Stanford NM, editors. Transformations: classical sculpture in colour. Copenhagen: Ny Carlsberg Glyptotek; 2014. p. 208–23.
9. Jeammet V. Tanagras: figurines for life and eternity: the Musée du Louvre's collection of Greek figurines. Valencia: Fundación Bancaja; 2010.
10. Pagès-Camagna S. Terracottas and colour. In: Jeammet V, editor. Tanagras: figurines for life and eternity: the Musée du Louvre's collection of Greek figurines. Valencia: Fundación Bancaja; 2010. p. 250–1.
11. Verri G. The application of visible-induced luminescence imaging to the examination of museum objects. In: Pezzati L, Salimbeni R, editors. Munich: SPIE; 2009. p. 739105–12.
12. Verri G, Opper T, Devièse T. The 'Treu Head': a case study in Roman sculptural polychromy. Br Mus Tech Bull. 2010;4:39–54.
13. Verri G. The spatially resolved characterisation of Egyptian blue, Han blue and Han purple by photo-induced luminescence digital imaging. Anal Bioanal Chem. 2009;394(4):1011–21.
14. Dyer J, Verri G, Cupitt J. Multispectral imaging in reflectance and photo-induced luminescence modes: a user manual. 2013. http://www.britishmuseum.org/pdf/charisma-multispectral-imaging-manual-2013.pdf. Accessed 03 Jan 2017.
15. Accorsi G, Verri G, Bolognesi M, Armaroli N, Clementi C, Miliani C, et al. The exceptional near-infrared luminescence properties of cuprorivaite (Egyptian blue). Chem Commun. 2009;23:3392–4.
16. Bracci S, Caruso O, Galeotti M, Iannaccone R, Magrini D, Picchi D, et al. Multidisciplinary approach for the study of an Egyptian coffin (late 22nd/early 25th dynasty): combining imaging and spectroscopic techniques. Spectrochim Acta Part A. 2015;145:511–22.
17. de la Rie ER. Fluorescence of paint and varnish layers (part I). Stud Conserv. 1982;27(1):1–7.
18. de la Rie ER. Fluorescence of paint and varnish layers (part II). Stud Conserv. 1982;27(2):65–9.
19. de la Rie ER. Fluorescence of paint and varnish layers (part III). Stud Conserv. 1982;27(3):102–8.
20. Blume C. Bright Pink, blue and other preferences. Polychrome hellenistic sculpture. In: Østergaard JS, Nielsen AM, Stanford NM, editors. Transformations: classical sculpture in colour. Copenhagen: Ny Carlsberg Glyptotek; 2014. p. 166–89.
21. Verri G, Comelli D, Cather S, Saunders D, Pique F, editors. Post-capture data analysis as an aid to the interpretation of ultraviolet-induced fluorescence images. San Jose: SPIE; 2008.
22. Verri G, Saunders D. Xenon flash for reflectance and luminescence (multispectral) imaging in cultural heritage applications. Br Mus Tech Bull. 2014;8:83–92.
23. Comelli D, Capogrosso V, Orsenigo C, Nevin A. Dual wavelength excitation for the time-resolved photoluminescence imaging of painted ancient Egyptian objects. Herit Sci. 2016;4(1):21.
24. Daveri A, Vagnini M, Nucera F, Azzarelli M, Romani A, Clementi C. Visible-induced luminescence imaging: a user-friendly method based on a system of interchangeable and tunable LED light sources. Microchem J. 2016;125:130–41.
25. Pozza G, Ajò D, Chiari G, De Zuane F, Favaro M. Photoluminescence of the inorganic pigments Egyptian blue, Han blue and Han purple. J Cult Herit. 2000;1(4):393–8.
26. Martinez K, Cupitt J. VIPS—a highly tuned image processing software architecture. In: IEEE international conference on image processing 2005; 11–14 September 2005; Genoa, Italy. p. 574–7.
27. Dyer J, Russell J. Analysis of pigment from a group of Hellenistic terracottas. Department of Conservation and Scientific Research Analytical Report 2012-88. London: British Museum; 2012
28. Daniels V, Devièse T, Hacke M, Higgitt C. Technological insights into madder pigment production in antiquity. Br Mus Tech Bull. 2014;8:13–28.
29. Claro A, Melo MJ, Schäfer S, de Melo JSS, Pina F, van den Berg KJ, et al. The use of microspectrofluorimetry for the characterization of lake pigments. Talanta. 2008;74(4):922–9.
30. Cardon D. Natural dyes. Sources, tradition, technology and science. London: Archetype Publications Ltd.; 2007.
31. de Graaff JHH, Roelofs WGT, Bommel MRV. The colourful past: origins, chemistry and identification of natural dyestuffs. Riggisberg: Abegg-Stiftung; 2004.
32. Kirby J, Spring M, Higgitt C. The technology of red lake pigment manufacture: study of the dyestuff substrate. Natl Gallery Tech Bull. 2005;26:71–87.
33. Derksen GCH, Lelyveld GP, van Beek TA, Capelle A, de Groot Æ. Two validated HPLC methods for the quantification of alizarin and other anthraquinones in *Rubia tinctorum* cultivars. Phytochem Anal. 2004;15(6):397–406.
34. Sanyova J. Étude des pigments organiques préparés à partir des racines des rubiacées européennes. In: Goupy J, Mohen J-P, editors. Art et chimie, la couleur. Paris: CNRS éd.; 2000. p. 14–7.
35. Wouters J, Vanden Berghe I, Richard G, Breniaux R, Cardon D. Dye analysis of selected textiles from three Roman sites in the Eastern desert of Egypt. Dyes Hist Archaeol. 2008;21:1–16.
36. Sanyova J, Reisse J. Development of a mild method for the extraction of anthraquinones from their aluminum complexes in madder lakes prior to HPLC analysis. J Cult Herit. 2006;7(4):229–35.
37. Fostiridou A, Karapanagiotis I, Vivdenko S, Lampakis D, Mantzouris D, Achilara L, et al. Identification of pigments in Hellenistic and roman funeral figurines. Archaeometry. 2016;58(3):453–64.
38. Clementi C, Doherty B, Gentili PL, Miliani C, Romani A, Brunetti BG, et al. Vibrational and electronic properties of painting lakes. Appl Phys A Mater Sci Process. 2008;92(1):25–33.
39. Clementi C, Miliani C, Verri G, Sotiropoulou S, Romani A, Brunetti BG, et al. Application of the Kubelka–Munk correction for self-absorption of fluorescence emission in carmine lake paint layers. Appl Spectrosc. 2009;63(12):1323–30.
40. Verri G, Clementi C, Comelli D, Cather S, Piqueé F. Correction of ultraviolet-induced fluorescence spectra for the examination of polychromy. Appl Spectrosc. 2008;62(12):1295–302.
41. Thoury M, Delaney JK, de la Rie ER, Palmer M, Morales K, Krueger J. Near-infrared luminescence of cadmium pigments: in situ identification and mapping in paintings. Appl Spectrosc. 2011;65(8):939–51.